Electronic Structure and Optical Properties of Mg_2Si, Mg_2Ge, and Mg_2Sn†

M. Y. Au-Yang*
Department of Physics, University of California, Berkeley, California 94720
AND
Marvin L. Cohen‡
Department of Physics and Inorganic Materials Division, Lawrence Radiation Laboratory, University of California, Berkeley, California 94720

(Received 13 August 1968)

The electronic band structure and optical constants of Mg_2Si, Mg_2Ge, and Mg_2Sn are calculated using the empirical pseudopotential method. The results are compared with experiment.

I. INTRODUCTION

THE empirical pseudopotential method[1] (EPM) has been used to calculate the band structures and optical constants of many different types of crystals[2–9] with much success. One advantage of using this method is that it yields optical constants which can be directly compared with optical measurements. Recently, good reflectance and electroreflectance data on the family of compounds Mg_2Si, Mg_2Ge, and Mg_2Sn were obtained by Scouler[10] and Vázquez *et al.*[11] We have, therefore, used the EPM to calculate the band structures and optical constants for these materials in an attempt to understand the optical structure.

Using potentials obtained in previous band-structure calculations, we have computed the electronic band structures for Mg_2Si, Mg_2Ge, and Mg_2Sn on a mesh of points in the Brillouin zone. From these points the imaginary part of the dielectric function $\epsilon_2(\omega)$ is obtained,[12] and from $\epsilon_2(\omega)$ the reflection coefficient is calculated. The derivative of the reflection coefficient is also obtained to compare with electroreflectance data.

Lee[13] and Folland[14] have previously calculated band structures for Mg_2Si, and Lee also gave the results for Mg_2Ge; however, neither calculation gives optical constants for these compounds, and the two results for Mg_2Si do not agree with each other. We have compared our results with these calculations and we have used a critical-point analysis of the interband energy contours to identify the structure in the $\epsilon_2(\omega)$ curves in terms of interband transitions. Our analysis shows that the previously existing calculations cannot yield optical constants that are consistent with experiment to within 1 eV. Our results, however, agree very well with experiment; the discrepancy between theory and experiment over the entire region of interest (0–10 eV) is within 0.4 eV for all three compounds.

We also found that the peak heights in our calculated optical spectrum agree well with experiment. The agreement is better than that obtained in more ionic crystals.[2–7] We believe that this agreement results from the lack of excitonlike binding between the electron hole pair because of the large static dielectric constants of these crystals.

This paper is divided into three sections. Section II discusses the pseudopotential Hamiltonian and the form factors. In Sec. III, the results are given and comparison with experiment is made in the following order: reflectance, electroreflectance, and energy gap measurements. Section III concludes with a comparison of our results with those of Lee and of Folland.

II. CALCULATIONS

The EPM involves the variation of pseudopotential form factors to fit optical data.[1] In this work, we imposed two further restrictions: The form factors were chosen to yield close agreement not only with optical data, but also with existing form factors for the individual constituent elements: the group-IV elements,[1,14] and Mg.[15] Furthermore, the same pseudopotential was used for the Mg ion in the three compounds. The success of the calculations indicates the correctness of associating a pseudopotential with an ion, independent of its chemical state. Screening effects should modify the

† Supported in part by the National Science Foundation.
* Present address: Research Laboratory, Eastman Kodak Company, Rochester, N. Y. 14615.
‡ Alfred P. Sloan Foundation Fellow.
[1] M. L. Cohen and T. K. Bergstresser, Phys. Rev. **141**, 789 (1966), and references therein.
[2] C. Fong, W. Saslow, and M. L. Cohen, Phys. Rev. **168**, 992 (1968).
[3] W. Saslow, T. K. Bergstresser, C. Y. Fong, and M. L. Cohen, Solid State Commun. **5**, 667 (1967).
[4] M. L. Cohen, in *Proceedings of the International Conference on II-VI Semiconducting Compounds, Providence, 1967*, edited by D. G. Thomas (W. A. Benjamin, Inc., New York, 1967), p. 462.
[5] T. K. Bergstresser and M. L. Cohen, Phys. Rev. **164**, 1069 (1967).
[6] P. J. Lin, W. Saslow, and M. L. Cohen, Solid State Commun. **5**, 893 (1967).
[7] C. Y. Fong and M. L. Cohen, Phys. Rev. Letters **21**, 22 (1968).
[8] D. Brust, J. C. Phillips, and F. Bassani, Phys. Rev. Letters **9**, 94 (1962).
[9] D. Brust, M. L. Cohen, and J. C. Phillips, Phys. Rev. Letters **9**, 389 (1962).
[10] W. J. Scouler, previous paper, Phys. Rev. **178**, 1353 (1969).
[11] F. Vázquez, R. A. Forman, and M. Cardona, Phys. Rev. **176**, 905 (1968).
[12] D. Brust, Phys. Rev. **134**, A1337 (1964).
[13] P. M. Lee, Phys. Rev. **135**, A1110 (1964).
[14] N. O. Folland, Phys. Rev. **158**, 764 (1967).
[15] A. O. E. Animalu and V. Heine, Phil. Mag. **12**, 1249 (1965).

TABLE I. Pseudopotential form factors (in Ry) for Mg_2X; $V_1=(\Omega_X/\Omega_{cell})V^X(|G|)$, $V_2=(2\Omega_{Mg}/\Omega_{cell})V^{Mg}(|G|)$, and G is in units of $2\pi/a$, where a is the side of the cube for the Mg_2X lattice.

			Mg_2Si		Mg_2Ge		Mg_2Sn	
G	$\|G^2\|$	$V(\|G\|)$	V^{Mg}	V^{Si}	V^{Mg}	V^{Ge}	V^{Mg}	V^{Sn}
(111)	3	V_1	···	−0.33	···	−0.34	···	−0.23
(200)	4	V_1-V_2	−0.03	−0.215	−0.03	−0.203	−0.045	−0.215
(220)	8	V_1+V_2	0.06	−0.015	0.06	−0.043	0.07	−0.01
(311)	11	V_1	···	0.039	···	0.035	···	0.02
(222)	12	V_1-V_2	0.04	0.055	0.04	0.05	0.049	0.02
(400)	16	V_1+V_2	0.025	0.079	0.025	0.052	0.035	0.006
(331)	19	V_1	···	0.056	···	0.01	···	0
(420)	20	V_1-V_2	0.01	0.04	0.01	0	0.015	0

pseudopotential, but the differences are expected to be small for similar nonmetallic compounds.

To calculate the band structure, we assume an energy-independent pseudopotential, so that the pseudo-Hamiltonian is

$$\mathcal{H}=-(\hbar^2/2m)\nabla^2+V(\mathbf{r}). \tag{1}$$

The weak pseudopotential is expanded in the reciprocal lattice

$$V(\mathbf{r})=\sum_{\mathbf{G}} V(\mathbf{G})e^{-i\mathbf{G}\cdot\mathbf{r}}, \tag{2}$$

where $\mathbf{G}$ is a reciprocal lattice vector. For the compounds Mg_2X, where X is Si, Ge, or Sn, the structure is cubic fluorite. The lattice is fcc with three atoms per primitive cell. The element X occupies a lattice site, and the magnesium atoms are at $\pm\mathbf{u}$, where $\mathbf{u}=(\frac{1}{4},\frac{1}{4},\frac{1}{4})a$, and a is the length of the cube. Thus we can write

$$\begin{aligned}V(\mathbf{G})&\equiv\frac{1}{\Omega_{cell}}\int_{cell} V(\mathbf{r})e^{i\mathbf{G}\cdot\mathbf{r}}d^3r\\&=\frac{1}{\Omega_{cell}}\Big(\int_X V^X(\mathbf{r})e^{i\mathbf{G}\cdot\mathbf{r}}d^3r\\&\quad+\sum_{p=\pm1}e^{ip\mathbf{u}\cdot\mathbf{G}}\int_{Mg}V^{Mg}(\mathbf{r})e^{i\mathbf{G}\cdot\mathbf{r}}d^3r\Big),\end{aligned} \tag{3}$$

where Ω_{cell} is the volume of the primitive cell. Writing $\mathbf{G}=(h,k,l)2\pi/a$, we have

$$\begin{aligned}V(\mathbf{G})=(1/\Omega_{cell})\{&\Omega_X V^X(\mathbf{G})+2\Omega_{Mg}V^{Mg}(\mathbf{G})\\&\times\cos[\tfrac{1}{2}\pi(h+k+l)]\},\end{aligned} \tag{4}$$

where Ω_X and Ω_{Mg} are the volume per atom of X and Mg, respectively; $V^X(\mathbf{G})$ and $V^{Mg}(\mathbf{G})$ are the corresponding pseudopotentials. We will assume spherically symmetric atomic pseudopotentials and thus $V(\mathbf{G})=V(|\mathbf{G}|)$.

Taking the pseudopotentials of Si, Ge, and Sn from Cohen and Bergstresser[1] (CB) and that of Mg from Animalu and Heine,[15] we find nonvanishing form factors only for $|G|^2\leq 20(2\pi/a)^2$. For the fcc lattice, there are eight such form factors. Using Eq. (4), we can write these form factors in terms of the atomic form factors, as shown in column 3 of Table I. We note that because the lattice constants of Mg_2X are different from the lattice constants of the elements, the values of the atomic pseudopotentials are obtained by interpolation from a smooth curve drawn from the known atomic pseudopotential form factors.

To calculate the optical properties from the band structure, we first calculate $\epsilon_2(\omega)$. To do this we use the expression

$$\begin{aligned}\epsilon_2(\omega)=\frac{e^2\hbar^2}{3\pi m^2\omega^2}\sum_{c,v}\int&\delta(E_c(\mathbf{k})-E_v(\mathbf{k})-\hbar\omega)\\&\times|\langle U_{\mathbf{k},v}|\nabla|U_{\mathbf{k},c}\rangle|^2d^3k,\end{aligned} \tag{5}$$

where c and v stand for conduction and valence bands, and $U_{\mathbf{k},n}$ is the periodic part of the nth band wave function. We approximate the exact $U_{\mathbf{k},n}$ by the eigenfunction of the pseudo-Hamiltonian, Eq. (1). The numerical evaluation of this expression for the fcc lattice is discussed elsewhere.[3]

The function $\epsilon_1(\omega)$ is obtained from $\epsilon_2(\omega)$ by using the Kramers-Kronig (KK) relations with an approximate tail function for $\omega>\omega_c$, where ω_c is the largest ω for which $\epsilon_2(\omega)$ is calculated. The reflection coefficient is obtained from $\epsilon_1(\omega)$ and $\epsilon_2(\omega)$.

III. RESULTS

The band structures obtained using the form factors in Table I for Mg_2Si, Mg_2Ge, and Mg_2Sn are shown in Figs. 1–3 for symmetry directions of the Brillouin zone. In Figs. 4–6 we plot the calculated and experimental $\epsilon_2(\omega)$ for the three compounds. The experimental $\epsilon_2(\omega)$ was obtained from reflectivity data by KK transformation. In Fig. 7 we plot the pseudopotential form factors used in the calculations for the group-IV elements and magnesium. For the group-IV elements we compare the form factors with those of CB. We see that for Si and Ge, a smooth curve can be drawn through the pseudopotential form factors used here and those of CB. However, for Sn, we were forced to change the pseudopotential of CB slightly. The differences in energy of 0.02 Ry, however, is smaller than the spin-orbit coupling energy for Sn which we neglected. For magnesium, we

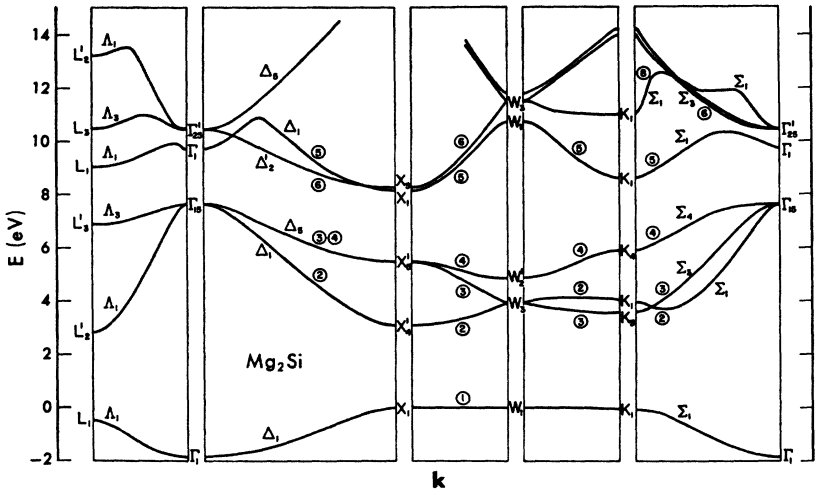

FIG. 1. Band structure of Mg_2Si.

compared our potential with the potential calculated by Animalu and Heine[15] and that used by Kimball, Stark, and Mueller.[16]

Inspection of Figs. 1–6 illustrates that the band structures and the $\epsilon_2(\omega)$ curves for the three compounds are similar. We shall first discuss their common features, and then discuss these band structures individually by comparison with reflectivity data (Sec. III B), electroreflectance data (Sec. III C), energy-gap measurements (Sec. III D), and the existing band-structure calculations of Lee and of Folland (Sec. III E).

A. Common Features

The valence-band maximum is at Γ, with symmetry Γ_{15}, and the conduction-band minimum is at X. The fundamental energy gap is thus indirect. The symmetry of the conduction-band minimum is either X_1 or X_3, but these two levels are close together. These features best exhibit themselves in electrical measurements.

The optical structure of these compounds can best be identified by a critical-point analysis. If one examines carefully the band structure and its associated $\epsilon_2(\omega)$ curve, it is possible to identify the interband transitions between valence and conduction states contributing to $\epsilon_2(\omega)$: The important transitions come from pairs of bands for which the joint density of states is near a singularity. The singular points of the zone are called critical points (cp's), and they give rise to structure in $\epsilon_2(\omega)$. An analysis of these cp's explains the general similarities of the $\epsilon_2(\omega)$ curves for the three compounds. For example, we find that the fourth and fifth bands along Σ, the fourth and sixth bands along Δ, and the fourth, fifth, and sixth bands along Λ are almost parallel over a large region of the zone for all the three compounds; thus the joint density of states is large there. Furthermore, the X_{4-6} gap is at about the same energy as the Σ_{4-5} cp. The main peak, which results mainly from the Σ_{4-5} transitions, thus has a large magnitude. Another important fact to notice is that the energy separation of the fourth and fifth bands along Λ is always below the main peak, whereas that of the fourth and sixth bands along Λ is always above. These

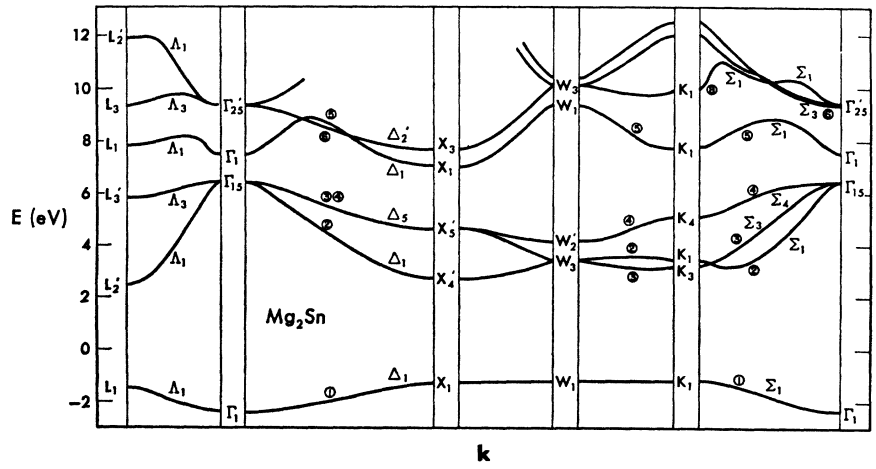

FIG. 2. Band structure of Mg_2Ge.

[16] J. C. Kimball, R. W. Stark, and F. M. Mueller, Phys. Rev. 162, 600 (1967).

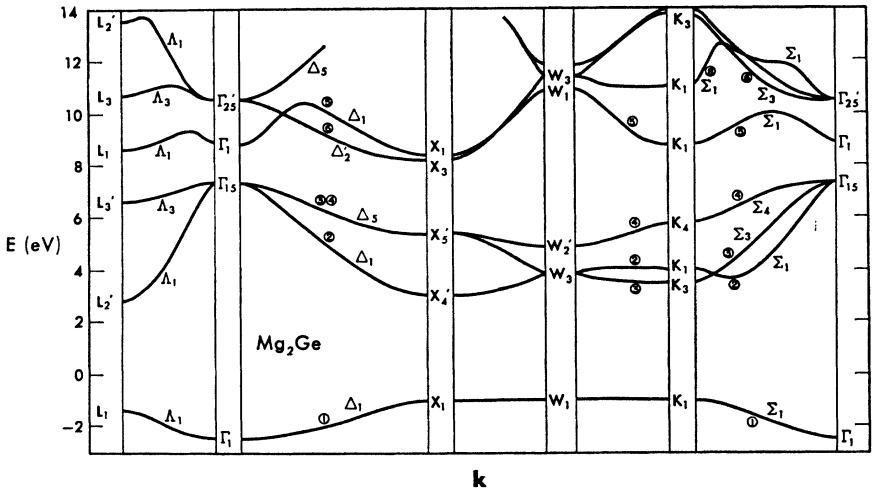

FIG. 3. Band structure of Mg_2Sn.

three main contributions to $\epsilon_2(\omega)$ therefore dictate the general three-peak shape of the $\epsilon_2(\omega)$ curve (though the first peak merges with the main peak in Mg_2Si and Mg_2Sn).

We shall next discuss the optical structure of each compound separately.

B. Reflectance

1. Mg_2Si (*Figs. 1 and 4*)

The experimental $\epsilon_2(\omega)$ curve starts with an indirect tail at about 0.6 eV. These indirect transition contributions are not included in the calculations, however: The theoretical $\epsilon_2(\omega)$ curve starts at 2.1 eV resulting from the $\Gamma_{15} \rightarrow \Gamma_1$ transition with an associated cp of M_0 symmetry. This structure can be identified with the sharp rise at about 2 eV in the experimental $\epsilon_2(\omega)$.

The following is a discussion of the major contributions to the theoretical $\epsilon_2(\omega)$; a comparison of the cp's in the experimental and theoretical $\epsilon_2(\omega)$ curves as a function of energy for all three compounds is given in Table II.

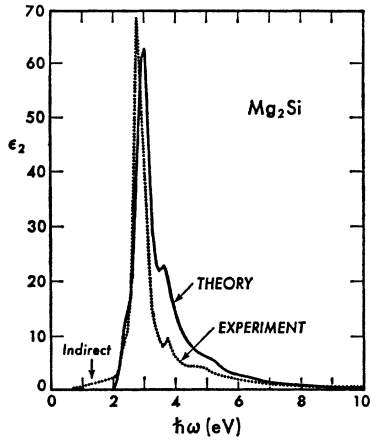

FIG. 4. Calculated and experimental imaginary part of the dielectric function $\epsilon_2(\omega)$ for Mg_2Si.

Above the threshold for the direct transition there is the 2.2-eV $L_3' \rightarrow L_1$ transition, which is closely followed by the 2.4-eV $\Lambda_3 \rightarrow \Lambda_1$ transition. The associated cp's have M_0 and M_3 symmetry, respectively. The main peak starts at about 2.6 eV; the transitions responsible are $X_5' \rightarrow X_1$, $X_5' \rightarrow X_3$, and $K_4 \rightarrow K_1$, all having M_0 symmetry. As stated earlier, the large region of the zone along Δ, the $\Delta_5 \rightarrow \Delta_2'$ transitions, gives a large contribution above the $X_5' \rightarrow X_3$ gap of 2.6 eV. The peak structure of the main peak is a result of M_2 and M_3 cp's arising from $\Sigma_4 \rightarrow \Sigma_1$ and $\Delta_5 \rightarrow \Delta_2'$ transitions, respectively, at about 3.0 eV.

Above the main peak the next structure is a peak at 3.7 eV which arises from $L_3' \rightarrow L_3$, and Λ_3-Λ_3 transitions of types M_2, M_3; Δ_5-Δ_1 transitions also contribute an M_3 in this region. Above this peak there are a large number of different regions in the zone contributing to $\epsilon_2(\omega)$. We can associate part of the contributions from 4.5–5 eV to the $\Delta_1 \rightarrow \Delta_1$, $K_1 \rightarrow K_1$, $K_3 \rightarrow K_1$, and $X_4' \rightarrow X_1$ transitions (see Table II). These contributions give rise to a bump at around 5 eV.

Inspection of Table II and Fig. 4 shows that there is good agreement between theory and experiment both

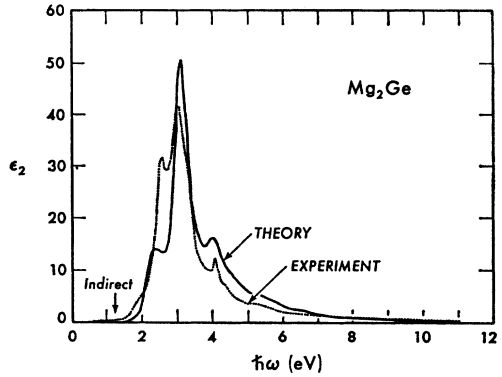

FIG. 5. Calculated and experimental imaginary part of the dielectric function $\epsilon_2(\omega)$ for Mg_2Ge.

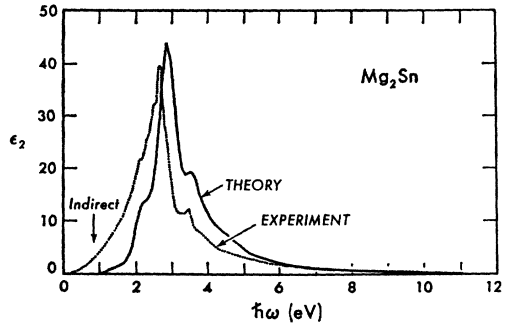

FIG. 6. Calculated and experimental imaginary part of the dielectric function $\epsilon_2(\omega)$ for Mg_2Sn.

for the magnitudes and positions in energy of the structure in $\epsilon_2(\omega)$. Even the last bump at 5 eV shows up well in the experimental curve.

2. Mg_2Ge (*Figs. 2 and 5*)

For Mg_2Ge the experimental indirect tail starts at 0.7 eV, which compares fairly well with our calculated value for the indirect gap of 0.92 eV. The theoretical threshold arises from the $\Gamma_{15} \rightarrow \Gamma_1$ transition at 1.5 eV with a cp of type M_0. At higher energies the M_0 and M_3 cp's arising from $L_3' \rightarrow L_1$ (2.0 eV) and the $\Lambda_3 \rightarrow \Lambda_1$ (2.2 eV) transitions contribute as in Mg_2Si. The main peak, however, does not start until about 2.9 eV, where we have an M_0 cp coming from $X_5' \rightarrow X_3$ transitions. The large separation in energy between the $L\Lambda$ contributions and the start of the main peak results in a $L\Lambda$ peak (Fig. 5) instead of a $L\Lambda$ shoulder (Fig. 4) as in the Mg_2Si case. The $\Delta_5 \rightarrow \Delta_2'$ transitions again contribute, but not as much as in the Mg_2Si case because these bands do not give a cp. The peak structure arises partially from M_0 cp's of the $K_4 \rightarrow K_1$ and $X_5' \rightarrow X_1$ transitions at 3.0 eV, and the main contribution comes from the M_2 cp of the $\Sigma_4 \rightarrow \Sigma_1$ transition. The M_3 cp of the $\Gamma_{15} \rightarrow \Gamma_{25}'$ transition is at 3.2 eV. The last peak, from 3.9 to 4.2 eV is again the result of $\Delta_5 \rightarrow \Delta_1$ (M_3), $L_3' \rightarrow L_3$ (M_2), and $\Lambda_3 \rightarrow \Lambda_3$ (M_3) transitions. Finally, we again have a group of cp contributions creating a bump at 5.2 eV.

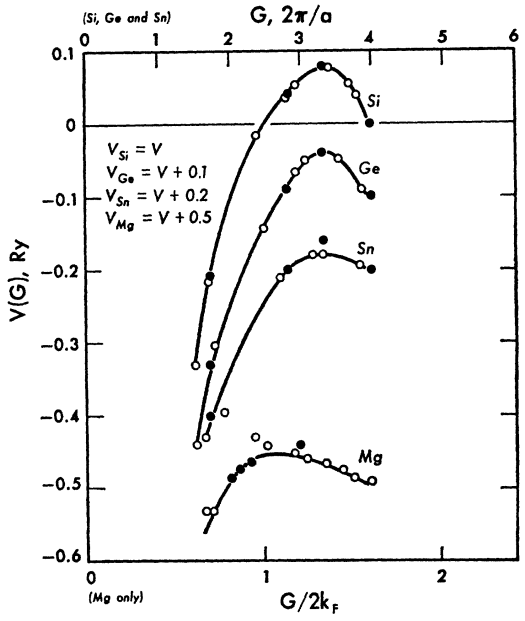

FIG. 7. Pseudopotentials of the elements Si, Ge, Sn, and Mg; a is the lattice constant for the semiconductor element and k_F is the Mg Fermi momentum. The open circles are the form factors used in the calculations. For Si, Ge, and Sn the closed circles are the form factors of CB. For Mg, the closed circles are the form factors of Kimball, Stark, and Mueller; the smooth curve is that of Animalu and Heine.

The comparison between theory and experiment can now be made by looking at Table II and Fig. 5. There is good agreement between the curves for the positions in energy of the structure in $\epsilon_2(\omega)$. However, the magnitude of the first $L\Lambda$ peak is appreciably bigger on the experimental curve. Although part of this discrepancy may have been the result of using pseudomatrix ele-

TABLE II. Calculated transition energies for Mg_2Si, Mg_2Ge, and Mg_2Sn and their identifications. The experimental transition energies, when identified, are shown in parentheses.

Transition	Type of singularity			Energy (eV)		
	Mg_2Si	Mg_2Ge	Mg_2Sn	Mg_2Si	Mg_2Ge	Mg_2Sn
$\Gamma_{15} \rightarrow \Gamma_1$	M_0	M_0	M_0	2.06 (2.1)	1.49 (1.6)	1.06
$L_3' \rightarrow L_1$	M_0	M_0	M_0	2.15	1.99 (2.1)	1.97
$\Lambda_3 \rightarrow \Lambda_1$	M_3	M_3	M_3	2.39	2.22	2.03
$X_5' \rightarrow X_1$	M_0	M_0	M_0	2.62 (2.5)	3.01	2.35 (2.3)
$\Delta_5 \rightarrow \Delta_2'$	M_3	no cp	no cp	2.81	...	...
$X_5' \rightarrow X_3$	M_0	M_0	M_1	2.74	2.84	3.02
$(K_4 \rightarrow K_1)_{45}$	M_0	M_0	M_0	2.74	3.03	2.69 (2.5)
$\Gamma_{15} \rightarrow \Gamma_{25}'$	M_0	M_3 or M_0	M_0	2.80	3.20	2.94
$\Sigma_4 \rightarrow \Sigma_1$	M_2	M_2	M_2	3.01 (2.7)	3.16 (3.0)	2.83 (2.7)
$L_3' \rightarrow L_3$	M_2	M_2	M_2	3.59 (3.7)	4.08 (4.1)	3.52 (3.4)
$\Lambda_3 \rightarrow \Lambda_3$	M_3	M_3	M_3	3.79	4.22	3.71
$\Delta_5 \rightarrow \Delta_1$	M_3	M_3	M_3	3.87	3.94	3.24
$(K_1 \rightarrow K_1)_{25}$	M_0	M_0	M_0	4.59	4.74	4.16
$\Delta_1 \rightarrow \Delta_1$	M_0	no cp	M_0	4.60	...	4.23
$\Delta_1 \rightarrow \Delta_1$	M_1	no cp	M_1	4.63	...	4.29
$X_4' \rightarrow X_1$	M_1	M_1	M_1	5.03	5.37	4.27
$(K_3 \rightarrow K_1)_{35}$	M_0	M_0	M_0	5.06	5.29	4.55

TABLE III. Electroreflectance structure and its comparison with theory between 1.5 and 4.5 eV. The identifications are also given. Some structure is found both in the theoretical and experimental curves; however, these do not appear to be associated with a single critical point.

	Mg_2Si		Mg_2Ge		Mg_2Sn	
Transition	Theor	Expt	Theor	Expt	Theor	Expt
$\Gamma_{15} \rightarrow \Gamma_1$	2.05	2.27	1.7	1.64	1.3	...
$\Lambda_3 \rightarrow \Lambda_1$	2.4	2.51	2.3	2.37	2.1	1.96
$X_5' \rightarrow X_1$	...	...	...	...	2.35	2.24
$K_4 \rightarrow K_1$	2.9	2.78	3.1	2.71	2.8	2.48
$\Sigma_4 \rightarrow \Sigma_1$	3.18	3.05	3.3	2.88	3.1	2.70
...	3.4	3.28	3.7	3.31	3.25	2.96
$\Lambda_3 \rightarrow \Lambda_3$	3.7	3.8	4.1	4.03	3.60	3.60
...	...	...	...	...	3.8	3.86

ments in the calculation of $\epsilon_2(\omega)$, the large experimental peak may have been caused by the tail function used in the KK transform of the reflectivity.[10] Finally, as for Mg_2Si, we again see the bump at 5.2 in the experimental $\epsilon_2(\omega)$.

3. Mg_2Sn (*Figs. 3 and 6*)

The experimental tail starts at a low value of 0.2 eV, which does not compare very favorably with our value of 0.64 eV for the indirect gap. However, the data were taken at 77°K, and at this temperature the fundamental gap should be almost 0.03 eV below its value at 0°K.[17] The discrepancy is therefore only about 0.4 eV.

The threshold for the direct transitions again arises from $\Gamma_{15} \rightarrow \Gamma_1$ transitions. The cp is of type M_0 and its energy value is 1.1 eV. Above this energy we have the usual $L\Lambda$ contributions at 2.0 eV which come from the M_0 and M_3 cp's from the $L_3' \rightarrow L_1$ and $\Lambda_3 \rightarrow \Lambda_1$ transitions, respectively. The $X_5' \rightarrow X_1$ and $K_4 \rightarrow K_1$ cp's, which in both the Mg_2Si and Mg_2Ge cases are coincident with either the $X_5' \rightarrow X_3$ cp or the main peak, are here distinct. These M_0 cp's are at 2.4 and 2.7 eV, respectively, thus creating two extra bumps on the low-energy side of the main peak. It is unfortunate that these fine points in the structure are smoothed out in the $\epsilon_2(\omega)$ plot and cannot be seen.

The main peak structure itself comes from $\Sigma_4 \rightarrow \Sigma_1$ transitions with an M_2 cp at 2.8 eV. The $\Delta_5 \rightarrow \Delta_2'$ transitions, as in the Mg_2Ge case, do not have a cp, and so the magnitude of the main peak is of the same size as that of Mg_2Ge and is appreciably smaller than that of Mg_2Si. The $\Delta_5 \rightarrow \Delta_2'$ transitions contribute mostly near Γ and X; the M_0 of $\Gamma_{15} \rightarrow \Gamma_{25}'$ at 2.9 eV and the M_1 of $X_5' \rightarrow X_3$ at 3 eV contribute to the main peak.

The last important peak is again a $L\Lambda$ peak, except here the $\Delta_5 \rightarrow \Delta_1$ contribution has moved down to the main peak, and so only $L_3' \rightarrow L_3$ (M_2, 3.5 eV) and $\Lambda_3 \rightarrow \Lambda_3$ (M_3, 3.7 eV) contribute. Above this peak we again have a group of cp contributions from about 4.2 to 4.6 eV creating a bump at about 4.4 eV.

A comparison of theory and experiment (Fig. 6 and Table II) shows good agreement in the positions of the principal structure in the $\epsilon_2(\omega)$. The larger magnitude of the experimental $\epsilon_2(\omega)$ on the low-energy side of the main peak can be attributed to the indirect transitions which we have neglected. They are more important here than in the previous cases because the indirect gap is much smaller here. Finally, we again find the bump (at 3.9 eV) above the last $L\Lambda$ peak in the experimental $\epsilon_2(\omega)$; however, in this case the agreement in energy between theory and experiment is not as good as in the previous cases. One factor which may be responsible for this discrepancy is our neglect of the spin-orbit coupling, which is larger for Sn than for either Ge or Si.

[17] U. Winkler, Helv. Phys. Acta **28**, 633 (1955).

TABLE IV. Calculated and experimental fundamental energy gaps for Mg_2Si, Mg_2Ge, and Mg_2Sn. Unless otherwise specified, these values are given for 0°K.

	Calc. indirect gap	Expt gap	Ref.
Mg_2Si	0.53	0.78	18
		0.80	21
		0.77	17
		0.69[a]	22
		0.65	10
Mg_2Ge	0.92	0.69	19
		0.74	17
		0.67[a]	22
		0.76	10
Mg_2Sn	0.64	0.33	20
		0.36	17
		0.23	10

[a] At 15°K.

C. Electroreflectance

While it is generally possible to see most of the cp's in the $\epsilon_2(\omega)$ curve, they show up much clearer in the first derivative of $\epsilon_2(\omega)$. The reason is that the slope of $\epsilon_2(\omega)$ at a cp is infinite. This derivative technique is used experimentally in electroreflectance measurements.

For the Mg_2X compounds, Vázquez *et al.*[11] have made electroreflectance measurements in the range 1.5–4.5 eV. We can make an approximate comparison between their data with our calculations by identifying the correspondence between the structure in the $\Delta R/R$ curve in the electroreflectance measurements with $(dR/d\omega)/R$ of our calculations. In Table III we tabulate the results. The agreement is seen to be good. Some of the structure missing in the $\epsilon_2(\omega)$ can easily be identified.

D. Energy-Gap Measurements

The fundamental gaps for these three compounds have been measured electrically and optically.[17–22] In Table IV we compare our results with experiment. The agreement is within 0.4 eV. We remark that for Mg_2Si

[18] R. G. Morris, R. D. Redin, and G. C. Danielson, Phys. Rev. **109**, 1909 (1958).
[19] R. D. Redin, R. G. Morris, and G. C. Danielson, Phys. Rev. **109**, 1916 (1958).
[20] R. F. Blunt, H. P. R. Frederikse, and W. R. Hosler, Phys. Rev. **100**, 663 (1955).
[21] M. W. Heller and G. C. Danielson, J. Phys. Chem. Solids **23**, 601 (1962).
[22] A. Stella and D. W. Lynch, J. Phys. Chem. Solids **25**, 1253 (1964).

we can raise the calculated gap to agree with experiment if we raise the energy of the main peak also. For Mg_2Ge and Mg_2Sn we notice that the gaps are both bigger than the experimental values, but since the spin-orbit interaction lowers these gaps, the agreement with experiment will be better if spin-orbit effects are included. The calculations show that the fundamental gaps are indirect; for Mg_2Si and Mg_2Ge, this appeared to be consistent with experiment.[23]

E. Comparison with Existing Calculations

If we compare our results with the two existing calculations for Mg_2Si, we find that our results are radically different from Folland's[14]; however, we find that Lee's[13] results are similar to ours with some shifts in the energies. The energy differences can be traced in part to the magnesium potential which was used in the two calculations. If we look at Fig. 7 and Table I, we see that there is considerable contribution from the magnesium potential for $|k|>2k_F$. However, in Lee's calculations an exponential tail function which vanishes at about $|k|=2.4$ a.u. for $|k|>2k_F$ was used. Thus Lee's effective pseudopotential [i.e., $V(|G|)$ in Table I] is bigger on the average, resulting in bigger energy differences. We would, therefore, expect an $\epsilon_2(\omega)$ curve derived from Lee's band to be similar to ours in shape, but the main structure would have higher energies compared with our result. Inspection shows that the shift in energy is about 1 eV.

In conclusion, we would say that our calculations quite successfully explain the data on Mg_2Si, Mg_2Ge, and Mg_2Sn. The band structures were calculated to fit optical structure using potentials which are consistent with those used in existing calculations for other crystals. We note that the minor structure in the measured optical spectra are also reproduced in the calculations.

ACKNOWLEDGMENTS

We would like to thank Dr. W. J. Scouler for allowing us to use his results prior to publication and Dr. Samuel Bowen for many helpful discussions.

[23] P. H. Koenig, D. W. Lynch, and G. C. Danielson, J. Phys. Chem. Solids **20**, 122 (1961).

PHYSICAL REVIEW VOLUME 178, NUMBER 3 15 FEBRUARY 1969

Longitudinal Anisotropy of the High-Field Conductivity of *n*-Type Germanium at Room Temperature

JOHN E. SMITH, JR.
IBM Watson Research Center, Yorktown Heights, New York 10598
(Received 7 October 1968)

New pulse measurements of the high-field conductivity of *n*-type germanium at room temperature have been performed. Contrary to previous measurements, the conductivity is anisotropic above the Ohmic field range. The highest current for a given field is found along the ⟨100⟩ crystallographic axes; the ⟨110⟩ current is as much as 9% lower, and the ⟨111⟩ current 14% lower than the ⟨100⟩ current. The maximum anisotropy is found at a field of 3 kV/cm. No region of constant drift velocity is found; current increases with field up to 30 kV/cm, the highest field applied.

1. INTRODUCTION

IN contrast to the situation in the low-field, Ohmic region, the magnitude of the current for a given high field is expected to, and has in general been found to depend on current direction in *n*-type Ge. Several measurements of the longitudinal anisotropy of the high-field conductivity of *n*-type Ge have been reported.[1–4] This anisotropy is a result of the many-valley conduction-band structure of Ge, and the effective-mass anisotropy of the individual valleys. The rate at which electrons absorb energy from the electric field depends on the relative orientations of the valley and field, being highest when the field is along an "easy," or low-mass direction of the particular valley. The high-field mobility is a decreasing function of electron temperature, so the rate at which the contribution of electrons in a particular valley to the total current deviates from Ohmic behavior depends on the orientation of that valley relative to the field. In the low-field region, the anisotropic parts of the single-valley conductivities cancel, and the total conductivity is a scalar. Since the single-valley mobilities have different field dependences, this cancellation does not continue into the high-field region, and the high-field conductivity is not, in general, isotropic.

The above discussion has implicitly assumed that the electrons are evenly distributed among the four equivalent ⟨111⟩ valleys of the conduction band, which is not necessarily true. This distribution can be shifted by equivalent intervalley scattering. In relatively pure Ge,

[1] R. Barrie and R. R. Burgess, Can. J. Phys. **40**, 1056 (1962).
[2] M. I. Nathan, Phys. Rev. **130**, 2201 (1963).
[3] V. Dienys and J. Pozhela, Phys. Status Solidi **17**, 769 (1966).
[4] M. Dienene, V. Dienys, and J. Pozhela, Lietuovos Fiz. Rinkinys **6**, 431 (1966).